Frontiers of Information Technology & Electronic Engineering
www.jzus.zju.edu.cn; engineering.cae.cn; www.springerlink.com
ISSN 2095-9184 (print); ISSN 2095-9230 (online)
E-mail: jzus@zju.edu.cn

Review:

Recent developments in novel silica-based optical fibers*

Ting-yun WANG[1], Fu-fei PANG[1], Su-juan HUANG[1], Jian-xiang WEN[1],
Huan-huan LIU[1], Li-bo YUAN[†‡2]

[1]*Key Laboratory of Specialty Fiber Optics and Optical Access Networks, Joint International Research Laboratory of Specialty Fiber Optics and Advanced Communication, Shanghai Institute for Advanced Communication and Data Science, Shanghai University, Shanghai 200444, China*

[2]*Photonics Research Center, Guilin University of Electronic Technology, Guilin 541004, China*

[†]E-mail: lbyuan@vip.sina.com

Received Jan. 9, 2019; Revision accepted Apr. 17, 2019; Crosschecked Apr. 17, 2019

Abstract: We have summarized our recent work in the area of novel silica-based optical fibers, which can be classified into two types: silica optical fiber doped with special elements including Bi, Al, and Ce, and micro-structured multi-core fibers. For element-doped optical fiber, the Bi/Al co-doped silica fibers could exhibit a fluorescence spectrum covering the wavelength range between 1000 and 1400 nm with a full width at half maximum (FWHM) of about 150 nm, which enables its use in fiber amplifiers and laser systems. The Ce-doped fiber's center wavelengths of excitation and emission are about 340 and 430 nm, respectively. The sapphire-derived fiber (SDF) with high alumina dopant concentration in the core can form mullite through heating and cooling with arc-discharge treatment. This SDF can be further developed for an intrinsic Fabry-Perot interferometric that can withstand 1200 °C, which allows it to be used in high-temperature sensing applications. Owing to the strong evanescent field, micro-structured multi-core fiber can be used in a wide range of applications in biological fiber optic sensing, chemical measurement, and interference-related devices. Coaxial-core optical fiber is another novel kind of silica-based optical fiber that has two coaxial waveguide cores and can be used for optical trapping and micro-particle manipulation by generating a highly focused conical optical field. The recent developments of these novel fibers are discussed.

Key words: Optical fiber; Fiber optic device; Silica-based special fiber
https://doi.org/10.1631/FITEE.1900017 **CLC number:** O439

1 Introduction

Optical fibers have prompted the further development of modern technology and raised people's living standard owing to its wide bandwidth, low loss, capability of long-haul transmission, light weight, anti-electromagnetic interference, etc. In particular, driven by optical communication and optical sensing, the design and fabrication of functional silica-based optical fibers, including both active and passive fibers, is of great interest. To improve the capacity of optical communications, functional active fibers are expected to emit light covering a broadband range. A variety of rare-earth elements have been attempted to dope the silica fibers (Dianov, 2012; Chu et al., 2016; Zhao et al., 2017). For optical sensing, on the one hand, the target application of optical fibers is prone to harsh environments, due to the lack of electrical counterparts (Liu et al., 2016; Rizzolo et al., 2016; Seng et al., 2017; Chen et al., 2018); on the other hand, micro-structured holey fibers with different hole arrangements have also attracted great interest for biological and chemical sensing for their inherent microfluidic channels in the fibers (Xie et al., 1986; Hautakorpi et al., 2008; Cheng et al., 2014; Yuan et al., 2015; Yang et al., 2018). In addition, some solid

‡ Corresponding author
* Project supported by the National Natural Science Foundation of China (Nos. 61735009, 61535004, and 61827819)
ORCID: Li-bo YUAN, http://orcid.org/0000-0002-2425-4553

micro-structured fibers with special core arrangements have shown a distinct technical advantage for optical micro-manipulation (Benabid et al., 2002; Yuan et al., 2008; Zhao et al., 2016; Deng et al., 2017).

In this paper, we have summarized our recent work on novel silica-based optical fibers including both active and passive fibers. To achieve spectral emission covering 1000–1400 nm, we have co-doped the Bi/Al elements in the silica fibers exhibiting a fluorescence spectrum with full width at half maximum (FWHM) of about 150 nm. Such a broad emission spectrum allows the Bi/Al co-doped silica fibers to be used as gain fiber in fiber amplifiers and laser systems. To achieve radiation detection, the silica fiber could be doped with Ce. Such Ce-doped fibers have center wavelengths of excitation and emission located at about 340 and 430 nm, respectively. In addition to active fibers, we have developed passive fibers with high alumina dopant concentration in the fiber core, called the sapphire-derived optical fiber (SDF). The SDF can form mullite through heating and cooling during arc discharge treatment. Sensors that can withstand up to 1200 °C can be developed by constructing the Fabry-Perot (FP) interferometer in SDF. Besides the above mentioned fibers with fiber material improvement, we have designed and fabricated micro-structured multi-core fiber and coaxial-core optical fiber (CCF). The micro-structured multi-core fiber is designed to have a strong evanescent field, which enhances its usefulness for the applications in biological fiber optic sensing and chemical measurement. The CCF is developed for optical trapping and micro-particle manipulation by generating highly focused conical optical field. The recent developments of these novelty fibers will be discussed.

2 Silica optical fiber with special doping

2.1 Bismuth-doped silica optical fiber

The current gain fibers including Yb- and Er-doped fibers have insufficient bandwidth for large-capacity optical transmission. Therefore, it is urgent to develop a wide band gain fiber. Bismuth oxide is a promising candidate for optical amplifiers in the second telecommunication window (Fujimoto and Nakatsuka, 2003; Wang et al., 2009). Specifically, a bismuth-doped (Bi-doped) optical fiber enabling luminescence from 1.1 to 1.8 μm shows great potential in the applications of fiber lasers and broadband light sources (Dvoyrin et al., 2006; Zhang et al., 2013). The traditional method of fabricating Bi-doped fiber is to use modified chemical vapor deposition (MCVD) associated with the solution doping technique (Dvoyrin et al., 2006). However, the uniformity of the doped materials cannot be guaranteed since they are easily volatized at high temperature, which limits the fiber performance. The atomic layer deposition (ALD) method is a chemical vapor deposition technique based on the sequential use of a self-terminating gas phase chemical process, which is a self-limiting surface reaction (Puurunen, 2005). Such an ALD technique shows advantages over the MCVD method including high doping concentration and dispersibility, as well as good uniformity (George, 2009). We have fabricated Bi/Al co-doped silica fibers for the first time by integrating ALD and MCVD techniques, and investigated their optical properties (Wen et al., 2015).

The fabrication of Bi/Al co-doped silica fibers involves the following four steps: (1) Using the MCVD process, a porous soot layer is deposited inside the silica substrate tube; (2) Using the ALD technique (TFS-200, Beneq, Finland), Bi and Al ions are deposited on the surface of the porous soot layer; (3) Using the MCVD collapsing process, germanium (Ge) is added as a dopant to form core layers, and thus a Bi/Al co-doped optical fiber preform with the Ge-doped higher index core is fabricated; (4) The preform is drawn into fibers with diameters of about 8.6 and 126 μm for the core and cladding, respectively (Fig. 1). The refractive index difference between the fiber cladding and core is 0.99%, which is recorded by a fiber refractive analyzer (S14, Photon Kinetics Inc., USA).

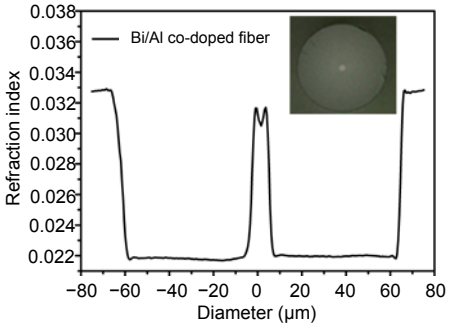

Fig. 1 Refractive index distribution of the Bi/Al co-doped silica optical fiber (The inset is the cross section)

Fluorescence spectra of the fabricated Bi/Al co-doped silica fiber with different pumping schemes are shown in Fig. 2. The length of the fiber under test is about 3 m. The pump power of the 980 nm laser reaches 195 mW. The fluorescence intensity becomes strong beyond 1000 nm and falls within the near-infrared region. The maximum peak of the fluorescence is located at 1084 nm, and exhibits a power level of –48 dBm. The FWHM of this peak is about 150 nm. To further increase the power level and the FWHM of fluorescence spectra, the pumping is chosen to be 1064 nm. Overall, the results obtained prove that the Bi/Al co-doped silica fiber fabricated using the ALD technique exhibits a fluorescence spectrum covering 1000–1400 nm with FWHM of about 150 nm; this allows it to be used as active fiber in the fiber amplifier and laser system.

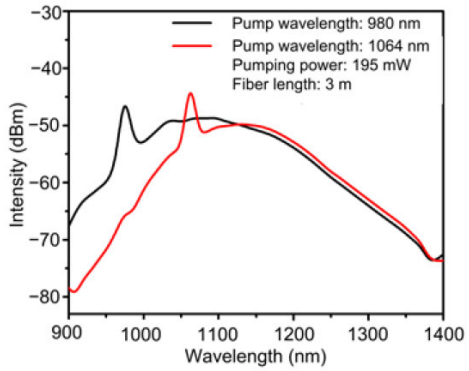

Fig. 2 Fluorescence spectra of Bi/Al co-doped silica fiber with 980-nm and 1064-nm pumping

2.2 Cerium-doped silica optical fiber

Ce^{3+} ions implemented as the luminescence center are widely used for various materials, such as crystal materials silicate and phosphate (Vedda et al., 2004; Koao et al., 2011). In traditional radiation detection, scintillators are often in bulk glasses, which makes remote radiation difficult to measure. Recently, Ce-doped fiber materials exhibit great potential for remote and real-time radiation measurement. However, the homogeneity and uniformity of single crystals are difficult to obtain in Ce-doped YAG/silica fiber and Ce^{3+} doped $YAlO_3$ crystal fiber using traditional methods including the rod-in-tube technique and the μ-pulling down technique (Alshourbagy et al., 2007; Liu et al., 2014). Ce-doped silica fiber materials show merits of radiation resistance, immunity to electromagnetic interference, low transmission loss, and low coupling loss of about 0.1 dB with the standard single mode fiber (Gherardi et al., 1993). In our study, a Ce-doped silica fiber with germanium dopants is fabricated using a powder-in-tube technique via the sol-gel method (Sun et al., 2017), and its excitation and emission spectra are measured and analyzed.

Figs. 3a and 3b show the images of Ce-doped fiber preform before and after drawing, respectively. The Ce-doped silica powder is fabricated using the sol-gel method (Sun et al., 2017). The microscopic images of the fiber cross section and fiber sample are shown in Figs. 3c and 3d, respectively. The diameter of the fiber core is about 6.3 μm and the outer cladding is about 120.7 μm. The difficulty in controlling the fiber diameter during fiber drawing is originated mainly from the stability of the heat source. A confocal micro Raman spectrometer (INVIA, Renishaw) is used to study the structure of the sol-gel powder and Ce-doped silica fiber before and after fiber drawing (Fig. 4). The bands (ω_1 and ω_3) at 437 and

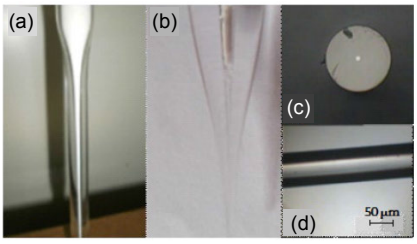

Fig. 3 Images of Ce-doped silica fiber fabricated using the powder-in-tube method

(a) and (b) are the Ce-doped fiber preform before and after drawing, respectively; (c) and (d) are the microscope images of the cross section and the side of a single fiber, respectively

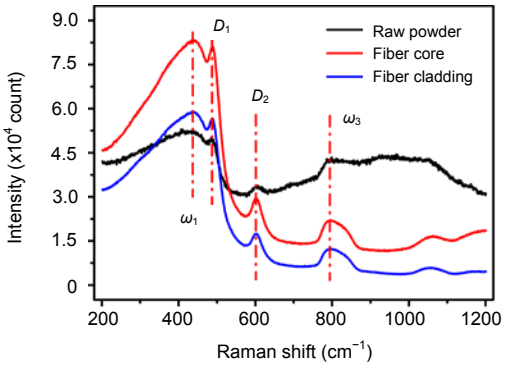

Fig. 4 Raman spectra of Ce-doped silica powder and the core and cladding of Ce-doped silica fiber

795 cm^{-1} are attributed to the symmetric stretching of bridging oxygen and Si-O-Si bending vibrations (Galeener, 1979). The two peaks at 488 and 602 cm^{-1} (D_1 and D_2) are conclusive features that appear in four- and three-membered ring structures of vitreous SiO_2, respectively (Pasquarello and Car, 1998). The results indicate that the core material of the fiber has already changed from silica powder to silica glass during the fiber drawing process, which is the same as the cladding silica glass.

The excitation and emission spectra are recorded using an Edinburgh FLS-980 spectrophotometer in the 200–800-nm wavelength region with Xe lamp excitation (Fig. 5). The center wavelengths of excitation and emission are located at about 340 and 430 nm, respectively. The excitation and emission peaks originate from the 5d-4f transition energy level of Ce^{3+}. The 4f energy level is less affected by the matrix materials because it is located in an inner layer. However, the 5d energy level is exposed to the electron outer shell. After heat treatment, the Ce^{3+} ions are no longer in the free state; instead, they are attached to the silica materials network structure, which results in the energy level of 5d shifting downward and being widened. Therefore, the emission peak of Ce-doped silica material is of a typical broadband spectrum.

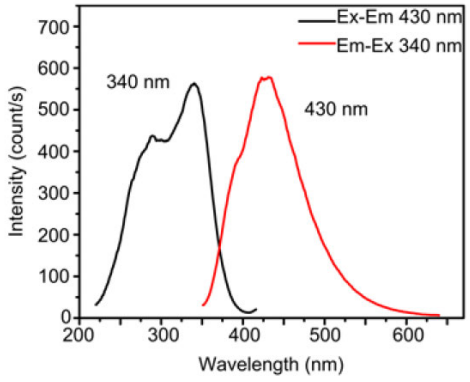

Fig. 5 Excitation and emission spectra of the Ce-doped silica fiber

2.3 Sapphire-derived optical fiber

Ultra-high-temperature sensing is important in turbine engines, power plants, and the petrochemical and gas industry. To withstand high temperatures and maintain high sensitivity, various fibers have been proposed, including fiber Bragg gratings, long-period gratings (LPGs), Mach-Zehnder interferometers, and FP interferometers. However, the performance degradation of the created structures limits the working temperature of the sensors. Sapphire optical fibers have drawn much attention for sensor development because of their high melting point and hardness (Wang et al., 1992). The interferometer-based sapphire fiber sensors for measuring the temperatures up to 1400 °C have been reported (Huang et al., 2015). Traditional sapphire fibers are all pure core structure without cladding confinement. Since a portion of light penetrates the surrounding, any containment on such large-core sapphire fiber might attenuate the light signal, and the performance of the sensors may be degraded in harsh environments. Recently, SDFs with a core-cladding structure have been widely developed (Dragic et al., 2012a, 2012b; Elsmann et al., 2014; Grobnic et al., 2015), showing advantages of high alumina dopant concentration, weak Brillouin scattering, good solubility of rare-earths, high mechanical strength, and mode confinement. Using SDF, we have demonstrated the application of the SDF-based intrinsic Fabry-Perot interferometer in high-temperature sensing.

The mass production of SDF can be achieved using the rod-in-tube method by inserting a sapphire rod into a quartz tube (Hong et al., 2017; Xu et al., 2017). The diameters of the core and cladding are measured to be 16 and 125 μm, respectively. The SDF has an alumina-silica (Al_2O_3-SiO_2) composite core with a high concentration of alumina of a mole fraction up to 32%. To create an FP interferometer on SDF, a new mechanism of refractive index modulation has been designed to form reflected mirrors. The refractive index of the fiber core increases along with the crystallization of mullite through heating and cooling during the arc discharge process (Hong et al., 2017; Xu et al., 2017). The selected discharge intensity is 16.6 mA and the discharge duration is 3 ms. The material modification of the alumina-silica composite core results from the rearrangement of core materials at near the splicing point where the arc-discharge occurs. Refractive index modulation up to 0.015 by crystallization can be achieved. By applying the crystalized SDF as a reflective mirror and the end facet as another mirror, the SDF-based FP interferometer is achieved, as shown in the inset of Fig. 6.

The SDF-based FP sensor developed is placed into a tube furnace for temperature sensing and the

maximum temperature up to 1200 °C is achieved. Fig. 6 gives the reflective spectrum of the FP interferometer at 1200 °C, showing that the extinction ratio of the interference spectrum is about 15 dB at 1550 nm. The free-spectrum range is about 10 nm, which corresponds to the cavity length of FP. Notably, the device can keep working at 1200 °C for several hours. Results show that the SDF-based FP sensor can be used in harsh environments such as turbine engines, power plants, and in petrochemical and gas industry.

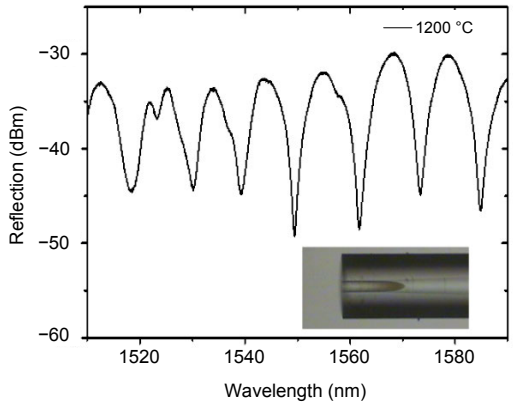

Fig. 6 Reflective spectrum of the SDF-based FP sensor during the constant temperature process at 1200 °C

3 Micro-structured optical fiber

Micro-structured fibers, such as photonic-crystal fiber and anti-resonant fiber, have attracted much attention in the last two decades (Russell, 2006; Poletti, 2014). The optical properties of micro-structure fibers are determined mainly by the air-hole structure of the cladding. The combination of micro-structured fiber and in-fiber integrated devices, for instance, fiber Bragg gratings, provides a platform for designing novel fiber optic components (Eggleton et al., 2001) and fiber optic sensors (Han et al., 2006; Jewart et al., 2006; Geernaert et al., 2008). In this section, we focus on the two kinds of refractive index-guiding fibers developed recently: multi-core polarization-maintaining fiber and CCF.

3.1 Multi-core polarization-maintaining fiber

Recently, hollow elliptical multi-core polarization-maintaining fiber has been found to be a new member of the family of suspended-core fibers (Guan et al., 2011; Tian et al., 2011). The fundamental mode of this fiber has a non-zero cutoff frequency and a low polarization birefringence with an order of magnitude of only 10^{-5}. The weak birefringence highly depends on the thickness of the thin cladding and the size of the central air hole. This allows this kind of fiber to have a strong evanescent field, and therefore enables its applications in biological fiber optic sensing, chemical measurement, and interference-related devices.

Fig. 7a shows a schematic of the structure and the refractive index profile of a hollow elliptical twin-core fiber. The optical fiber has a large central air hole with a diameter of 65 μm, two elliptical cores with long and short axes of $2a$=7.2 μm and $2b$=3.0 μm, respectively. The ellipticity e=$2b$/($2a$)=0.42. The diameter of the outer optical fiber cladding is 125 μm. The refractive indices of the fiber cladding, fiber core, and air hole are represented by n_d, n_c, and n_a, respectively, where n_c>n_d>n_a=1. Between the fiber-core layer and the air hole, there is a thin quartz inner coating with thickness d=1 μm. The high-order mode cutoff wavelength of the fiber is 0.934 μm. The shape of the elliptical core structure diagram is shown in Fig. 7b. Owing to the existence of this thin cladding layer, the evanescent wave field in the cladding layer can partially leak into the air hole. When the air holes are filled with liquid or solid material, the filled material can change the effective refractive index of the area around the core. Therefore, this kind of fiber can be used to develop biochemical sensors based on the fiber evanescent field. In addition, because the fiber has the characteristics of an elliptic core fiber, it will have geometric birefringence, which gives the fiber a certain polarization-maintaining function. Moreover, its unique multi-core structure can be used to make various in-fiber interferometers. Similarly, the cross sections of hollow elliptical three- and four-core polarization-maintaining fibers are shown in Fig. 7c.

3.2 Coaxial-core optical fiber

CCF is another kind of novelty fiber that has two coaxial waveguide cores: one round core in the center and one circular core surrounding the round core in the cladding. It is well known that the optical fibers containing only one circular core have been applied for optical-vortex generation and mode-division-multiplexing, owing to their attractive characteristics

such as large effective area, weak mode coupling between adjacent azimuthal modes, and nearly identical gain for all guided signal modes (Yan et al., 2012; Jin et al., 2016; Zhu et al., 2018). These applications are based on the separation of the degenerate modes in the circular core. Another application of the circular-core fiber is for optical trapping and micro-particle manipulation by generating a highly focused conical optical field (Yu et al., 2012; Deng et al., 2015). We have developed an optical fiber tweezer based on the circular-core fiber and accomplished three-dimensional trap with only one single fiber (Zhu et al., 2018). However, this type of tweezer has only the capture function, and cannot perform other operations on the captured particles simultaneously.

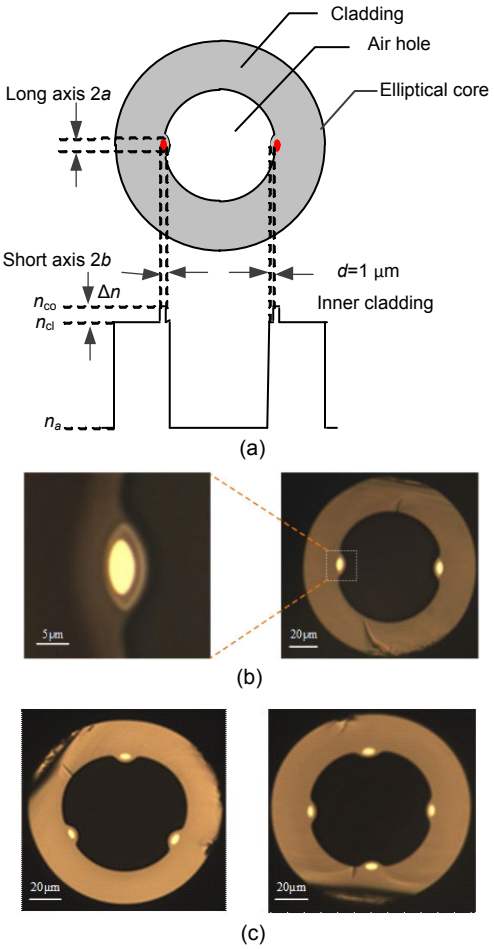

Fig. 7 Schematic of the structure and refractive index profile of the hollow elliptical twin-core fiber (a), the shape of the elliptical core structure diagram (b), and the cross section of the hollow elliptical three- and four-core polarization-maintaining fiber (c)

To improve the manipulation performance of the circular-core fiber based optical tweezers, we have designed and manufactured the CCF (Deng et al., 2017). As an application result, a novel all-fiber device that integrates a stable 3D optical tweezer by using the circular core and a long-distance lightwave guide for small particle moving under the control of one single fiber was fabricated in the CCF (Zhang et al., 2013). In addition to the particle-trapping function, the all-fiber device is able to shoot small particles along the central lightwave guide.

The cross section and refractive index distribution of the CCF are shown in Figs. 8a and 8b, respectively. The refractive indices and geometric size of both the center and circular cores can be designed according to practical demands. The light beams in the two cores independently transmit along the fiber. To achieve the multifunction of the CCF, one end of the CCF is polished to a shape of a cone frustum. For an annular light beam propagating in the circular core of the CCF, a total internal reflection will occur as it reaches the core-medium interface, and a highly focused ring beam is formed at the outside of the cone frustum. In the center core of the CCF, a Gaussian beam is injected, which is output directly from the cone frustum while maintaining a Gaussian distribution. When the radiation force on the micro-particle caused by the output Gaussian beam exceeds the negative trapping force of the focus ring beam, the trapped particle will escape from the optical gradient force potential well and move along the Gaussian beam. As a result, two different micro-particle manipulating functions are achieved on a single CCF: trapping micro particles with the focused ring beam from the circular core and shooting micro-particles with the Gaussian beam by the center core of the CCF. Detailed descriptions of trapping applications with

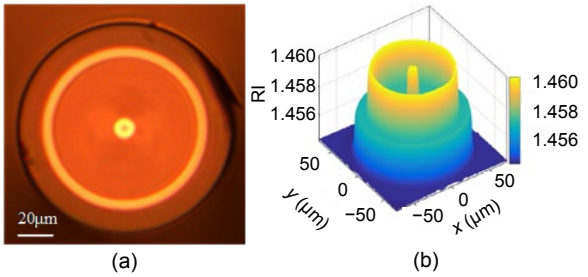

Fig. 8 The cross-section image (a) and 3D refractive index profile (b) of the CCF

the CCF fiber can be found in the literature (Yu et al., 2012; Deng et al., 2017).

4 Conclusions

We have developed two kinds of novel fibers, active element-doped silica optical fibers and passive micro-structured fibers, which can be used in a wide range of applications in optical communication, optical sensing, and micro-manipulation. We have accomplished active fibers including Bi/Al co-doped silica fibers exhibiting a fluorescence range of 1000–1400 nm with FWHM of about 150 nm and the Ce-doped silica fibers with excitation and emission wavelengths of about 340 and 430 nm, respectively. Sapphire-derived fiber was realized to construct a Fabry-Perot interferometer with high mechanical strength for ultra-high-temperature measurement. Multi-core polarization maintaining fibers, including the microfluidic channel and optical transmission channel in one fiber, were also produced for applications in biological sensing, chemical measurement, and polarization interference devices. Coaxial-core optical fiber, which is promising for micro-particle manipulation, was demonstrated to develop a multi-functional optical micro-manipulation device.

References

Alshourbagy M, Bigotta S, Herbert D, et al., 2007. Optical and scintillation properties of Ce^{3+} doped $YALO_3$ crystal fibers grown by μ-pulling down technique. *J Cryst Growth*, 303(2):500-505. https://doi.org/10.1016/j.jcrysgro.2007.01.024

Benabid F, Knight JC, Russell PJSt, 2002. Particle levitation and guidance in hollow-core photonic crystal fiber. *Opt Expr*, 10(21):1195-1203. https://doi.org/10.1364/OE.10.001195

Chen H, Buric M, Ohodnicki PR, et al., 2018. Review and perspective: sapphire optical fiber cladding development for harsh environment sensing. *Appl Phys Rev*, 5(1): 011102. https://doi.org/10.1063/1.5010184

Cheng TL, Kanou Y, Deng DH, et al., 2014. Fabrication and characterization of a hybrid four-hole $AsSe_2$-As_2S_5 microstructured optical fiber with a large refractive index difference. *Opt Expr*, 22(11):13322-13329. https://doi.org/10.1364/OE.22.013322

Chu YS, Jing R, Zhang JZ, et al., 2016. Ce^{3+}/Yb^{3+}/Er^{3+} triply doped bismuth borosilicate glass: a potential fiber material for broadband near-infrared fiber amplifiers. *Sci Rep*, 6:33865. https://doi.org/10.1038/srep33865

Deng HC, Qi CC, Zhang XT, et al., 2015. Highly focused conical optical field for pico-newton scale force sensing. *J Lightw Technol*, 33(12):2486-2491. https://doi.org/10.1109/JLT.2014.2377118

Deng HC, Zhang Y, Yuan TT, et al., 2017. Fiber-based optical gun for particle shooting. *ACS Photon*, 4(3):642-648. https://doi.org/10.1021/acsphotonics.6b01010

Dianov EM, 2012. Bismuth-doped optical fibers: a challenging active medium for near-IR lasers and optical amplifiers. *Light Sci Appl*, 1(5):e12. https://doi.org/10.1038/lsa.2012.12

Dragic P, Ballato J, Ballato A, et al., 2012a. Mass density and the brillouin spectroscopy of aluminosilicate optical fibers. *Opt Mater Expr*, 2(11):1641-1654. https://doi.org/10.1364/OME.2.001641

Dragic P, Hawkins T, Foy P, et al., 2012b. Sapphire-derived all-glass optical fibres. *Nat Photon*, 6(9):627-633. https://doi.org/10.1038/nphoton.2012.182

Dvoyrin VV, Mashinsky VM, Bulatov LI, et al., 2006. Bismuth-doped-glass optical fibers—a new active medium for lasers and amplifiers. *Opt Lett*, 31(20):2966-2968. https://doi.org/10.1364/OL.31.002966

Eggleton BJ, Kerbage C, Westbrook PS, et al., 2001. Microstructured optical fiber devices. *Opt Expr*, 9(13):698-713. https://doi.org/10.1364/OE.9.000698

Elsmann T, Lorenz A, Yazd NS, et al., 2014. High temperature sensing with fiber Bragg gratings in sapphire-derived all-glass optical fibers. *Opt Expr*, 22(22):26825-26833. https://doi.org/10.1364/OE.22.026825

Fujimoto Y, Nakatsuka M, 2003. Optical amplification in bismuth-doped silica glass. *Appl Phys Lett*, 82(19):3325. https://doi.org/10.1063/1.1575492

Galeener FL, 1979. Band limits and the vibrational spectra of tetrahedral glasses. *Phys Rev B*, 19(8):4292-4297. https://doi.org/10.1103/PhysRevB.19.4292

Geernaert T, Luyckx G, Voet E, et al., 2008. Transversal load sensing with fiber Bragg gratings in microstructured optical fibers. *IEEE Photon Technol Lett*, 21(1):6-8. https://doi.org/10.1109/LPT.2008.2007915

George SM, 2009. Atomic layer deposition: an overview. *Chem Rev*, 110(1):111-131. https://doi.org/10.1021/cr900056b

Gherardi L, Marelli P, Serra A, et al., 1993. Radiation effects on doped silica-core optical fibers. *Nucl Phys B*, 32:436-440. https://doi.org/10.1016/0920-5632(93)90057-D

Grobnic D, Mihailov SJ, Ballato J, et al., 2015. Type I and II Bragg gratings made with infrared femtosecond radiation in high and low alumina content aluminosilicate optical fibers. *Optica*, 2(4):313-322. https://doi.org/10.1364/OPTICA.2.000313

Guan CY, Tian FJ, Dai Q, et al., 2011. Characteristics of embedded-core hollow optical fiber. *Opt Expr*, 19(21): 20069-20078. https://doi.org/10.1364/OE.19.020069

Han YG, Lee YJ, Kim GH, et al., 2006. Transmission characteristics of fiber Bragg gratings written in holey fibers

corresponding to air-hole size and their application. *IEEE Photon Technol Lett*, 18(16):1783-1785. https://doi.org/10.1109/LPT.2006.880762

Hautakorpi M, Mattinen M, Ludvigsen H, 2008. Surface-plasmon-resonance sensor based on three-hole microstructured optical fiber. *Opt Expr*, 16(12):8427-8432. https://doi.org/10.1364/OE.16.008427

Hong L, Pang FF, Liu HH, et al., 2017. Refractive index modulation by crystallization in sapphire-derived fiber. *IEEE Photon Technol Lett*, 29(9):723-726. https://doi.org/10.1109/LPT.2017.2682194

Huang J, Lan XW, Song Y, et al., 2015. Microwave interrogated sapphire fiber Michelson interferometer for high temperature sensing. *IEEE Photon Technol Lett*, 27(13): 1398-1401. https://doi.org/10.1109/LPT.2015.2422136

Jewart C, Chen KP, McMillen B, et al., 2006. Sensitivity enhancement of fiber Bragg gratings to transverse stress by using microstructural fibers. *Opt Lett*, 31(15):2260-2262. https://doi.org/10.1364/OL.31.002260

Jin XQ, Gomez A, Shi K, et al., 2016. Mode coupling effects in ring-core fibers for space-division multiplexing systems. *J Lightw Technol*, 34(14):3365-3372. https://doi.org/10.1109/JLT.2016.2564991

Koao LF, Swart HC, Obed RI, et al., 2011. Synthesis and characterization of Ce^{3+} doped silica (SiO_2) nanoparticles. *J Lumin*, 131(6):1249-1254. https://doi.org/10.1016/j.jlumin.2010.10.038

Liu B, Yu ZZ, Hill C, et al., 2016. Sapphire-fiber-based distributed high-temperature sensing system. *Opt Lett*, 41(18):4405-4408. https://doi.org/10.1364/OL.41.004405

Liu CN, Huang YC, Lin YS, et al., 2014. Fabrication and characteristics of Ce-doped fiber for high-resolution OCT source. *IEEE Photon Technol Lett*, 26(15):1499-1502. https://doi.org/10.1109/LPT.2014.2327127

Pasquarello A, Car R, 1998. Identification of Raman defect lines as signatures of ring structures in vitreous silica. *Phys Rev Lett*, 80(23):5145-5147. https://doi.org/10.1103/PhysRevLett.80.5145

Poletti F, 2014. Nested antiresonant nodeless hollow core fiber. *Opt Expr*, 22(20):23807-23828. https://doi.org/10.1364/OE.22.023807

Puurunen RL, 2005. Surface chemistry of atomic layer deposition: a case study for the trimethylaluminum/water process. *J Appl Phys*, 97(12):121301. https://doi.org/10.1063/1.1940727

Rizzolo S, Marin E, Morana A, et al., 2016. Investigation of coating impact on OFDR optical remote fiber-based sensors performances for their integration in high temperature and radiation environments. *J Lightw Technol*, 34(19):4460-4465. https://doi.org/10.1109/JLT.2016.2552459

Russell PSJ, 2006. Photonic-crystal fibers. *J Lightw Technol*, 24(12):4729-4749. https://doi.org/10.1109/JLT.2006.885258

Seng F, Stan N, King R, et al., 2017. Optical sensing of electric fields in harsh environments. *J Lightw Technol*, 35(4): 669-676. https://doi.org/10.1109/JLT.2016.2631149

Sun XX, Wen JX, Guo Q, et al., 2017. Fluorescence properties and energy level structure of Ce-doped silica fiber materials. *Opt Mater Expr*, 7(3):751-759. https://doi.org/10.1364/OME.7.000751

Tian FJ, Yuan LB, Dai Q, et al., 2011. Embedded multicore hollow fiber with high birefringence. *Appl Opt*, 50(33): 6162-6167. https://doi.org/10.1364/AO.50.006162

Vedda A, Chiodini N, Di Martino D, et al., 2004. Ce^{3+}-doped fibers for remote radiation dosimetry. *Appl Phys Lett*, 85(26):6356. https://doi.org/10.1063/1.1840127

Wang AB, Gollapudi S, Murphy KA, et al., 1992. Sapphire-fiber-based intrinsic Fabry-Perot interferometer. *Opt Lett*, 17(14):1021-1023. https://doi.org/10.1364/OL.17.001021

Wang TY, Zeng XL, Wen JX, et al., 2009. Characteristics of photoluminescence and Raman spectra of INP doped silica fiber. *Appl Surf Sci*, 255(17):7791-7793. https://doi.org/10.1016/j.apsusc.2009.04.179

Wen JX, Wang J, Dong YH, et al., 2015. Photoluminescence properties of Bi/Al-codoped silica optical fiber based on atomic layer deposition method. *Appl Surf Sci*, 349:287-291. https://doi.org/10.1016/j.apsusc.2015.04.138

Xie HM, Dabkiewicz P, Ulrich R, et al., 1986. Side-hole fiber for fiber-optic pressure sensing. *Opt Lett*, 11(5):333-335. https://doi.org/10.1364/OL.11.000333

Xu J, Liu HH, Pang FF, et al., 2017. Cascaded Mach-Zehnder interferometers in crystallized sapphire-derived fiber for temperature-insensitive filters. *Opt Mater Expr*, 7(4): 1406. https://doi.org/10.1364/OME.7.001406

Yan HW, Zhang ET, Zhao BY, et al., 2012. Free-space propagation of guided optical vortices excited in an annular core fiber. *Opt Expr*, 20(16):17904-17915. https://doi.org/10.1364/OE.20.017904

Yang XH, Zhao QK, Qi XX, et al., 2018. In-fiber integrated gas pressure sensor based on a hollow optical fiber with two cores. *Sens Actuat A*, 272:23-27. https://doi.org/10.1016/j.sna.2018.01.055

Yu Z, Liu ZH, Yang J, et al., 2012. A non-contact single optical fiber multi-optical tweezers probe: design and fabrication. *Opt Commun*, 285(20):4068-4071. https://doi.org/10.1016/j.optcom.2012.06.025

Yuan LB, Liu ZH, Yang J, et al., 2008. Twin-core fiber optical tweezers. *Opt Expr*, 16(7):4559-4566. https://doi.org/10.1364/OE.16.004559

Yuan TT, Zhong X, Guan CY, et al., 2015. Long period fiber grating in two-core hollow eccentric fiber. *Opt Expr*, 23(26):33378-33385.

https://doi.org/10.1364/OE.23.033378

Zhang JZ, Sathi ZM, Luo YH, et al., 2013. Toward an ultra-broadband emission source based on the bismuth and erbium co-doped optical fiber and a single 830nm laser diode pump. *Opt Expr*, 21(6):7786-7792. https://doi.org/10.1364/OE.21.007786

Zhao HY, Farrell G, Wang PF, et al., 2016. Investigation of particle harmonic oscillation using four-core fiber integrated twin-tweezers. *IEEE Photon Technol Lett*, 28(4): 461-464. https://doi.org/10.1109/LPT.2015.2499309

Zhao QC, Luo YH, Wang WY, et al., 2017. Enhanced broadband near-IR luminescence and gain spectra of bismuth/erbium co-doped fiber by 830 and 980 nm dual pumping. *AIP Adv*, 7(4):045012. https://doi.org/10.1063/1.4981903

Zhu L, Zhu GX, Wang AD, et al., 2018. 18 km low-crosstalk OAM + WDM transmission with 224 individual channels enabled by a ring-core fiber with large high-order mode group separation. *Opt Lett*, 43(8):1890-1893. https://doi.org/10.1364/OL.43.001890